Unmixing of multispectral photoacoustic images

Aneline DOLET[1,2], Rita AMMANOUIL[3], François VARRAY[1], Yubin LIU[4], Zhen YUAN[4], Piero TORTOLI[2], André FERRARI[3], Cédric RICHARD[3], Didier VRAY[1],

[1]Laboratoire CREATIS, Université Claude Bernard Lyon 1, France

[2]Department of Information Engineering, University of Florence, Florence, Italy

[3]Laboratoire Lagrange, Université de Nice Sophia-Antipolis, Nice, France

[4]Bioimaging Core, Faculty of Health Sciences, University of Macau, People's Republic of Macau, China

[1]aneline.dolet@creatis.insa-lyon.fr

Résumé – L'imagerie photoacoustique est une modalité hybride qui permet d'imager les tissus biologiques. L'illumination d'une zone d'intérêt par des impulsions laser à différentes longueurs d'onde permet d'obtenir une technique d'imagerie fonctionnelle car l'absorption optique des tissus est spécifique à la longueur d'onde utilisée. Pour différentes applications médicales, l'analyse d'images photoacoustiques multispectrales par la quantification du sang oxygéné (HbO2) et désoxygéné (Hb) dans les tissus est intéressante. Celle-ci peut être réalisée en utilisant les cartes d'abondance issues de méthodes de démélange. Ici, des méthodes de démélange, Group Lasso with Unit sum and Positivity constraints (GLUP) et Fully Constrained Least-Square (FCLS), utilisées dans le domaine hyperspectrale, sont mises en oeuvre pour quantifier des images photoacoustiques multispectrales. Les résultats de cette étude sont présentés sur deux jeux de données synthétiques et un jeu de données expérimentales. Ceux-ci montrent que ces méthodes permettent de quantifier des images photoacoustiques multispectrales avec de bonnes performances.

Abstract – Photoacoustic imaging is an hybrid modality to image biological tissues. Using multispectral optical excitation, photoacoustic imaging allows to obtain functional images due to the fact that a tissue has a specific optical absorption depending on the used wavelengths. Quantification of multispectral photoacoustic images can be of great interest to different applications by quantifying oxygenated (HbO2) and deoxygenated (Hb) blood in tissue. Quantification can be done by examining the abundance maps resulting from unmixing methods. Two hyperspectral unmixing methods, namely Group Lasso with Unit sum and Positivity constraints (GLUP) and Fully Constrained Least-Square (FCLS), are used to quantify multispectral photoacoustic images. Experiments using two synthetic and one experimental dataset show that unmixing methods provide good quantification performances, which is of great interest for various medical applications.

1 Introduction

Photoacoustic imaging is a medical imaging modality which couples optical and acoustic imaging [1]. It is based on the detection of acoustic pressure waves produced by a medium subject to a pulsed laser illumination locally increasing its temperature. The thermal expansions of optical absorbers create acoustic waves that propagate through the media to the surface where they are detected. Acquiring photoacoustic images of a region of interest at different wavelength bands provides a multispectral (3D) image where a pixel is endowed with a spectrum. Each tissue has a specific spectrum due to the fact that optical absorption depends on the light's illumination wavelength. For example, the spectral responses of oxygenated (HbO2) and deoxygenated (Hb) blood are mostly different in the range from 600 to 900 nm [2]. The study of the spectral evolution and the quantification of blood oxygenation in tissues is beneficial in various medical applications. This quantification is of great interest for various medical applications such as the diagnosis of malignant/benign tumors, the follow-up of carcinoma, and the evaluation of tissues death to cite a few [3].

Spectral unmixing, widely used in remote sensing [4], can be naturally extended to quantify multispectral photoacoustic data. The mixing framework distinguishes between a pure spectra (the endmembers) associated with pure materials, and mixed spectra which are usually a weighted mixture of the pure spectra. Three consecutive tasks are required for unmixing : determining the number of pure spectra, estimating their spectral signatures and their proportions (abundances) for each pixel. The pipeline VD [5], followed by N-FINDR [6] and FCLS [7] is among the most widely used to perform unmixing. We propose to use a blind and fully constrained approach known as the Group Lasso with Unit sum and Positivity constraints (GLUP) [8] for estimating the endmembers, and the Fully Constrained Least Squares (FCLS) method for estimating the abundances. We use this pipeline to quantify blood concentration in multispectral photoacoustic images.

The paper is organized as follows. Section 2 introduces the linear mixing model. Section 3 gives an overview of GLUP and FCLS. Finally, section 4 presents simulations with synthetic and real experimental photoacoustic dataset.

2 Linear mixing model

In multispectral imaging, a region of interest is imaged at different wavelength bands. Each pixel in the image is characterized by a spectrum which is the collection of acquired intensity values at each wavelength band. A pixel's spectrum is either pure and referred to as an endmember, or mixed i.e. composed of a mixture of the endmembers. Assume that the multispectral image is estimated at L wavelength bands, and contains in total N pixels indexed by $n = 1, \ldots, N$. According to the linear mixing model (LMM) [4], a mixed pixel is a convex combination of the endmembers. More formally, we have :

$$\boldsymbol{s}_n \quad = \sum_{i=1}^{M} a_{in} \boldsymbol{r}_i + \boldsymbol{e}_n, \, \forall \, n = 1, \ldots N, \tag{1}$$

where $\boldsymbol{s}_n \in \mathbb{R}^L$ is the L-dimensional spectrum for the n-th pixel, M denotes the number of endmembers, $a_{i,n}$ is the abundance of the i-th endmember in the n-th pixel, $\boldsymbol{r}_i$ is the L-dimensional spectrum of the i-th endmember, $\boldsymbol{e}_n$ is a vector of Gaussian white noise accounting for sensor noise and error of the model. All vectors are column vectors. Being contributions, the abundances must be positive and sum to one :

$$\begin{cases} a_{in} \geq 0, \\ \sum_{i=1}^{M} a_{in} = 1. \end{cases} \tag{2}$$

The LMM is a simple yet very representative model which was extensively studied in remote sensing, see for example the survey in [4]. For medical applications, the LMM can be a powerful tool for quantifying media like the oxygenation of blood in tissues. More precisely, the aim of this work is to use unmixing in order to quantify the concentration of blood in different inclusions. In this context, a spectrum is assumed to be either fully concentrated or diluted. The LMM can be naturally extended to this scenario, where the spectra of fully concentrated blood are regarded as pure spectra and their concentrations in diluted spectra are regarded as abundances. However, the sum-to-one constraint should be relaxed given that a mixed spectrum can be a diluted version of the endmember, for example it can be equal to 50% of the endmember. This can be done by simply adding a zero endmember in the LMM also known as a shadow endmember.

3 Unmixing pipeline

In the experiments, GLUP [8] and FCLS [7] were used to estimate the endmembers and the abundances respectively. In what follows, we briefly introduce the concepts of these two methods. GLUP assumes that the endmembers are unknown but present in the image, among the observations. Given this assumption, and without loss of generality, the linear mixing model (1) can be reformulated as follows :

$$\boldsymbol{s}_n \quad = \sum_{i=1}^{N} x_{in} \boldsymbol{s}_i + \boldsymbol{e}_n, \, \forall \, n = 1, \ldots N. \tag{3}$$

Similarly as above, x_{in} is the abundance of $\boldsymbol{s}_i$ in $\boldsymbol{s}_n$. On the one hand, if $\boldsymbol{s}_i$ is an endmember, the row $\boldsymbol{x}_{\lambda_i}$ of the matrix $\boldsymbol{X}$ whose elements are defined as $X_{in} = x_{in}$ for $i, n = 1, \ldots, N$ has non-zero entries and represents the corresponding abundance map. On the other hand, if $\boldsymbol{s}_i$ is a mixed pixel, $\boldsymbol{x}_{\lambda_i}$ has all its elements equal to zero. As a consequence, $\boldsymbol{X}$ admits $N - M$ rows of zeros, the other rows being equal to rows of $\boldsymbol{A}$. The premise in GLUP is that $\boldsymbol{X}$ allows to identify the endmembers in $\boldsymbol{S}$ through its non-zero rows. This property is exploited in GLUP in order to find the endmembers among the observations. The unmixing problem under investigation, requires that $\boldsymbol{X}$ only has a few rows different from zero, in addition to the non-negativity and sum-to-one constraints which leads to the following convex optimization problem :

$$\begin{array}{ll} \min_{\boldsymbol{X}} & \frac{1}{2} \sum_{i=1}^{N} \|\boldsymbol{S} - \boldsymbol{S}\boldsymbol{X}\|_{\mathrm{F}}^2 + \mu \sum_{k=1}^{N} \|\boldsymbol{x}_{\lambda_k}\|_2 \\ \text{subject to} & x_{ij} \geq 0 \quad \forall \, i, j \\ & \sum_{i=1}^{N} x_{ij} = 1 \quad \forall \, j, \end{array} \tag{4}$$

with $\mu \geq 0$ a regularization parameter, and $\boldsymbol{S} = [\boldsymbol{s}_1, \ldots, \boldsymbol{s}_N]$ is the observations matrix. The first term in (4) is the data fidelity term ensuring that the observations match model (3), and the second term is the Group Lasso regularization which induces sparsity in by possibly driving several rows of $\boldsymbol{X}$ to zero [9]. The constraints ensure that the abundances obey the positivity and the sum-to-one constraints. The resulting optimization is solved using a primal dual method, the readers are referred to [8] for more details. In conclusion, GLUP allows to identify the endmembers in $\boldsymbol{S}$ by identifying the non-zero rows in $\boldsymbol{X}$. Note that GLUP also provides the abundances estimated which correspond to the non-zero rows in the estimated matrix $\boldsymbol{X}$. However, similarly to [8], given the endmembers estimated by GLUP, FCLS is then used to estimate the abundances. FCLS solves a problem similar to problem (4) with $\mu = 0$ and using the estimated endmembers matrix rather than the observations matrix. FCLS allows to have a better estimation of the abundances, given that the endmembers are known at this stage and that the resulting optimization problem is better conditioned compared to problem (4).

4 Experimental results

4.1 Datasets description

We tested the proposed unmixing pipeline with two synthetic and one experimental dataset. The first synthetic dataset can be assimilated into three blood inclusions on a background. Two inclusions were simulated using one pure endmember (media) each (e.g. Hb and HbO2), and a third inclusion using an equal mixture (50% of each endmember). The endmembers are shown in Figure 1. The abundances at the boundaries of each inclusion are attenuated in order to have a light diffusion effect. In the second synthetic data set, we also simulate three inclusions. Two inclusions are constituted of one pure media each (e.g. ink and blood), and the third inclusion is synthetized using one of the endmember with half its intensity (i.e. with a concentration of 50%). The three spectra used to create

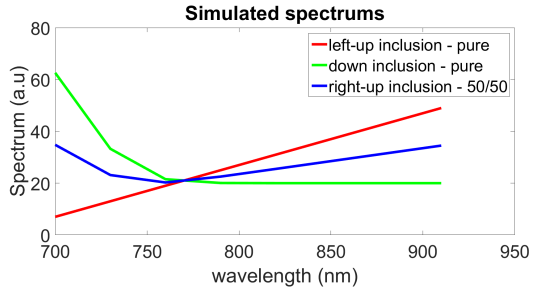

FIGURE 1 – Simulated spectrums used to create the three inclusions in the first synthetic dataset : the red and green spectra correspond to the endmembers, and the blue spectra corresponds to 50% of each endmember.

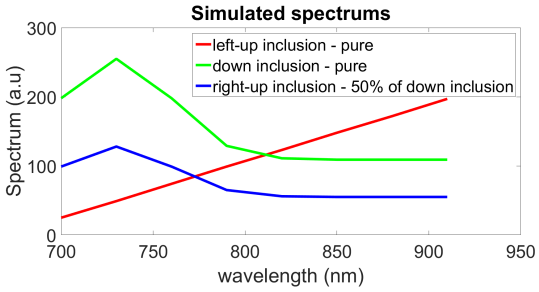

FIGURE 2 – Simulated spectrums used to create the three inclusions in the second synthetic dataset : the red and green spectra correspond to the endmembers, and the blue spectra corresponds to 50% of the green endmember.

this data set are shown in Figure 2. The decreasing coefficients are also applied on this dataset.

The proposed approach was also tested on a real experimental dataset acquired at the University of Macau with the multispectral photoacoustic tomography (PAT) acquisition scheme [10] in Figure 3. Figure 4 shows the phantom used which consists of a cylindrical PVA phantom with three spherical inclusions. Two inclusions are filled with two different concentrations of blood and the third one is filled with diluted black China ink (the right-up inclusion). The images are acquired at 8 different wavelengths from 700 to 910 nm with 30 nm steps.

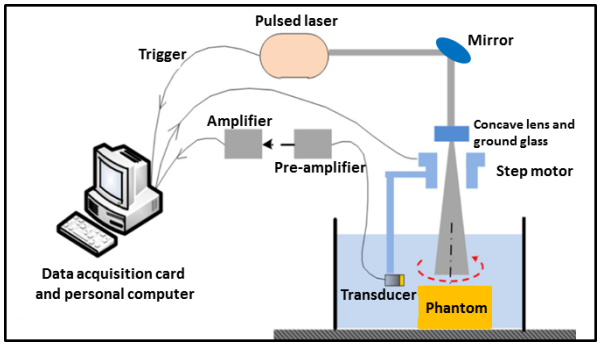

FIGURE 3 – Experimental setup for the photoacoustic tomography acquisitions.

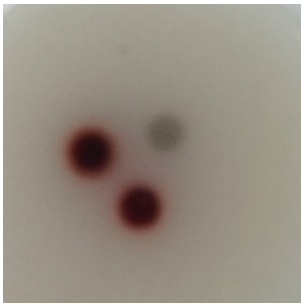

FIGURE 4 – Phantom used for the acquisitions, the inclusion in grey is the China ink inclusion, and the two dark red inclusions are the blood inclusions.

4.2 Unmixing pipeline

Before applying GLUP and FCLS, a pre-processing step is applied in order to discriminate the background from the region of interest. Given that the background has a low photoacoustic response, a threshold is applied in order to keep the pixels with higher photoacoustic signal as the region of interest. The retained pixels spectra are used with GLUP in order to identify the endmembers among these observations. Note that GLUP does not require the knowledge of the number of endmembers to be extracted a-priori. Given that in our experiments, the number of endmembers is known to be equal to 2, we kept the first two endmembers returned by GLUP. The endmembers estimated by GLUP in addition to the shadow endmember are then used with FCLS in order to estimate the abundances.

4.3 Results

Figures 5 and 6 show the endmembers obtained using GLUP and the abundance maps obtained using FCLS for the three datasets respectively. The first, second and third row in Figure 6 represent the abundance maps obtained with the first synthetic dataset, the second synthetic dataset and the real experimental dataset respectively. In each row, the first two columns correspond to the abundance maps of the non-zero endmembers whereas the third column corresponds to the shadow endmember abundance map. The unmixing results obtained with the first synthetic dataset (first row in Figure 6) show that the left-up inclusion and the bottom inclusion consist of two different endmembers (abundances at the inclusion center are equal to 1) whereas the right-up inclusion consists of an equal mixture of these two endmembers (abundances at the inclusion center are equal to 0.5). The unmixing results obtained with the second synthetic data set (second row in Figure 6) show that the right-up and the bottom inclusions consist of the same medium at different concentrations, approximately 0.5 and 1 respectively, whereas the left-up inclusion consists of another medium. Finally, the third row in Figure 6 shows the abundance maps obtained with the experimental data set. It can be seen that the left-up inclusion consists of one endmember, and that the other two inclusions (the right-up and the bottom one) consist of a second endmember. In all the previous cases, the third abundance

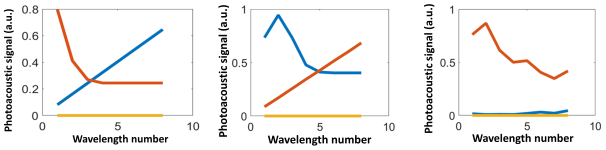

FIGURE 5 – Endmembers obtained by GLUP and the shadow (zero) endmember. From left to right : first synthetic data set, second synthetic dataset, and experimental dataset.

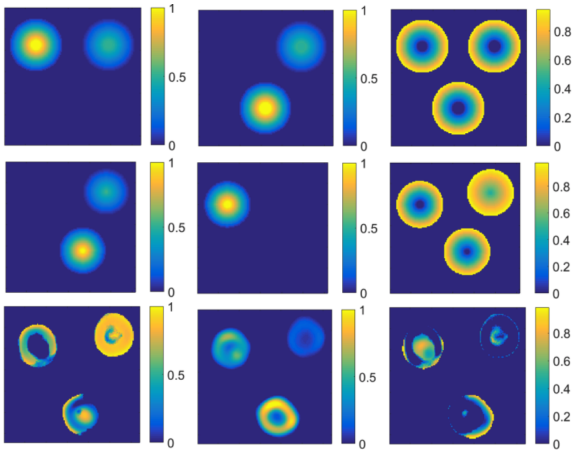

FIGURE 6 – Each row shows the abundance maps given by FCLS obtained with from top to bottom : first synthetic data set, second synthetic dataset, and experimental dataset.

map corresponds to the zero endmember where the abundances are mostly close to one at the boundaries accounting for the light diffusion effect.

Given that in all cases we had two endmembers representing media and the shadow one. We used then the first two abundance maps as the red and green components of an RGB image (Fig. 7) giving an intuitive and fast interpretation of the result. The first image in Figure 7 shows a red and a green inclusion corresponding to two different media, and a third greenish inclusion which is a mixture of these two media. The second image shows a green and two red inclusions at different intensities corresponding to the same media at different concentrations. Finally, the last image shows one red inclusion and two green ones at different intensities. In the latter case, the green inclusions are surrounded by a red boundary. This is due to the fact that the spectrum corresponding to the red endmember is very close to zero (see Figure 5).

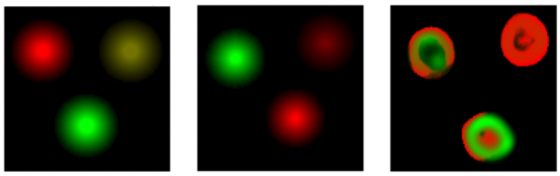

FIGURE 7 – Quantification maps obtained by using the abundance maps as the RGB images. From left to right : first synthetic data set, second synthetic dataset, and experimental dataset.

5 Conclusion and perspectives

In this work, we extended the use of GLUP and FCLS, originally used in remote sensing, to the medical domain. In particular, this unmixing pipeline was used to quantify multispectral photoacoustic images. In order to allow interpreting the abundances as concentrations we added a shadow endmember to the endmembers estimated by GLUP and estimated the abundances using FCLS. Experiments with synthetic and experimental datasets showed that the proposed pipeline was able to successfully quantify media's concentrations. As future work, it could be interesting to test the proposed approach on multispectral photoacoustic acquisitions of biological tissue such as meat and study the temporal evolution of the quantification as the tissue become stale.

6 Acknowledgements

This work was supported by the LABEX CELYA (ANR-10-LABX-0060) and LABEX PRIMES (ANR-10-LABX-0063) of Université de Lyon, within the program "Investissements d ?Avenir" (ANR-11-IDEX-0007) operated by the French National Research Agency (ANR). It was also performed within the framework of the Université Franco-Italienne (VINCI 2016) and the Région Rhône-Alpes (CMIRA 2016 - EXPLORA DOC).

References

[1] M. Vallet, F. Varray, M. Azizian, J. Boutet, and D. Vray, "Enhancement of photoacoustic imaging quality by using cmut technology : experimental study," in *IEEE International Ultrasonics Symposium Proceedings*, 2014, pp. 1296–1299.

[2] E. Hill, W. Xia, D. Nikitichev, K. Gurusamy, P. Beard, D. Hawkes, B. Davidson, and A. Desjardins, "Interventional multi-spectral photoacoustic imaging in laparoscopic surgery," in *SPIE*, 2016, vol. 9708.

[3] D. Bauer, R. Olafsson, L. Montilla, and R. Witte, "In vivo multi-modality photoacoustic and pulse echo tracking of prostate tumor growth using a window chamber," in *Society of Photo-Optical Instrumentation Engineers (SPIE)*, 2010.

[4] N. Keshava and J. F. Mustard, "Spectral unmixing," *IEEE Signal Processing Magazine*, vol. 19, no. 1, pp. 44–57, 2002.

[5] C. Chang and Q. Du, "Estimation of number of spectrally distinct signal sources in hyperspectral imagery," *IEEE Transactions on Geoscience and Remote Sensing*, vol. 42, no. 3, pp. 608–619, March 2004.

[6] M. E. Winter, "N-FINDR : an algorithm for fast autonomous spectral endmember determination in hyperspectral data," in *Proc. of the SPIE Imaging Spectrometry*, October 1999.

[7] D. C. Heinz and C. I. Chang, "Fully constrained least squares linear spectral mixture analysis method for material quantification in hyperspectral imagery," *IEEE Transactions on Geoscience and Remote Sensing*, vol. 39, no. 3, pp. 529–545, March 2001.

[8] R. Ammanouil, A. Ferrari, C. Richard, and D. Mary, "Blind and fully constrained unmixing of hyperspectral images," *IEEE Transactions on Image Processing*, vol. 23, no. 12, pp. 5510 – 5518, October 2014.

[9] M. Yuan and Y. Lin, "Model selection and estimation in regression with grouped variables," *Journal of the Royal Statistical Society : Series B (Statistical methodology)*, vol. 68, no. 1, pp. 49–67, February 2006.

[10] S. Li, B. Montcel, Z. Yuan, W. Liu, and D. Vray, "Multigrid-based reconstruction algorithm for quantitative photoacoustic tomography," in *Biomedical optics express*, 2015, vol. 6, pp. 2424–2434.